

LETTERS

InGaN solar cells with regrown GaN homojunction tunnel contacts

To cite this article: Ehsan Vadiee et al 2018 Appl. Phys. Express 11 082304

View the article online for updates and enhancements.

Related content

- Reduced-droop green III-nitride lightemitting diodes utilizing GaN tunnel junction
- Abdullah I. Alhassan, Erin C. Young, Ahmed Y. Alyamani et al.
- Polarization-enhanced InGaN/GaN-based hybrid tunnel junction contacts to GaN p-n diodes and InGaN LEDs
 Asad J. Mughal, Erin C. Young, Abdullah I. Alhassan et al.
- <u>Hybrid tunnel junction contacts to</u>
 <u>III-nitride light-emitting diodes</u>
 Erin C. Young, Benjamin P. Yonkee, Feng
 Wu et al.

InGaN solar cells with regrown GaN homojunction tunnel contacts



Ehsan Vadiee^{1,2}, Evan A. Clinton¹, Heather McFavilen³, Alex S. Weidenbach¹, Zachary Engel¹, Christopher Matthews¹, Chaomin Zhang², Chantal Arena³, Richard R. King², Christiana B. Honsberg², and W. Alan Doolittle¹

Received June 6, 2018; accepted July 9, 2018; published online July 27, 2018

Highly doped GaN p-n tunnel junction (TJ) contacts to InGaN solar cells are demonstrated, in which the TJs were grown by molecular beam epitaxy on top of active solar cell regions grown by metalorganic chemical vapor deposition. The effects of Si and Mg doping concentrations on solar cell characteristics are studied and used to improve turn-on voltage and series resistance. The highest doped cell with a TJ has an open-circuit voltage of 2.2 V, similar to that of the control cell fabricated using indium tin oxide (ITO), and a far less short-circuit current density loss from unwanted photogeneration in the TJ contact than in the ITO contact. © 2018 The Japan Society of Applied Physics

he III–nitride material system has outstanding importance for photonic and electronic devices, second only to silicon in the volume of its many applications. Recently, attention has been drawn to the design and fabrication of indium gallium nitride (InGaN) solar cells^{1,2)} owing to their unique properties, such as suitability for high-temperature operation, high radiation resistance,³⁾ high absorption coefficient, and tunable bandgap covering the entire visible solar spectrum.

A significant remaining challenge in III-nitride-based devices is the lack of low-resistance contacts to p-type GaN, owing to a low hole carrier concentration (N_A) and a high hole effective mass. A successful demonstration of GaN tunnel junctions (TJs) would have broad applications in optoelectronics since they convert p-type contact regions to n-type ones, which have low contact resistance. The reverse-biased and low-forward-biased TJ exhibits an ohmic behavior rather than rectification, providing a highly conductive path from an n-type layer to a p-type layer, resulting in a lower series resistance in light-emitting diodes (LEDs). This means that the TJ can be used for efficient hole injection into the p-type region of LEDs and can reduce the efficiency droop commonly observed in InGaN-based LEDs, which mainly originates from the asymmetric carrier transport properties of the n-type side (low activation energy) and p-type side (high activation energy). 4,5) GaN-based TJs were also successfully implemented in vertical-cavity surface-emitting lasers to achieve buried tunnel junctions for carrier confinements. 6) In this work, TJs operating in forward bias are demonstrated for the first time to achieve good carrier extraction in InGaN-based solar cells to overcome the low p-GaN lateral conductivity issue. In addition, TJs can potentially interconnect multiple solar cells with different indium mole fractions and bandgaps, providing a path for multijunction solar cells with higher efficiencies.

To increase the lateral conductivity of the p-GaN contact layer of an InGaN solar cell and address the thermal degradation of the active region, an indium tin oxide (ITO) cladding layer has been used. However, adding an ITO on p-GaN can introduce more complications for device fabrication. A highly doped GaN TJ can be an alternative to reduce the voltage drop due to current spreading and increase light absorption in the active region. Thus, the TJ can be used in solar cells to provide a low-resistivity n-type ohmic contact instead of a resistive p-type contact.

Different approaches have been demonstrated to achieve tunneling in GaN-based materials. Polarization-assisted

heterojunction tunnel diodes such as GaN/InGaN/GaN and GaN/AlN/GaN have been shown, in which a large internal electric field is created across the junctions owing to polarization dipoles to increase the tunneling probability. ^{8,9)} It was demonstrated that the GaN/InGaN/GaN TJ can reach a low specific resistance of $\sim\!10^{-4}\,\Omega\,\mathrm{cm}^2.^{10)}$ However, the heterojunction tunnel diode design is suboptimal for solar cells owing to a high absorption loss introduced by the InGaN layer and a low current density owing to the large bandgap of insulating AlN. Defect-assisted tunneling by introducing midgap states in the depletion region was also investigated but resulted in a high overall resistance and a low device reliability. ^{11,12)} Thus, a successful demonstration of a p–n GaN homojunction tunnel contact is desirable to overcome the mentioned drawbacks.

Metalorganic chemical vapor deposition (MOCVD) has shown an improved LED contact resistance using GaN homojunction tunnel contacts in place of the p-contact, but multiple attempts have been unsuccessful to demonstrate low-resistance stand-alone p-n GaN homojunction tunnel diodes. 13,14) The fundamental challenges associated with MOCVD growth, such as a low Mg activation efficiency in p-GaN, the Mg memory effect, and the hydrogen passivation of Mg, impose a substantial constraint on TJ growth. However, the aforementioned challenges do not exist in plasmaassisted molecular beam epitaxy (PAMBE) growth. Recently, GaN p-n TJs have been successfully realized by PAMBE showing negative differential resistance and intrinsic reverse Zener characteristics. 15,16) In particular, owing to the absence of hydrogen (H) in PAMBE, the p-GaN layers are not passivated by H atoms, eliminating the need for activation annealing. Additionally, a minimal Mg memory effect and a favorable low-temperature chemistry for Mg incorporation on substitutional sites lead to high hole concentrations in excess of $1.2 \times 10^{20} \,\mathrm{cm}^{-3}$ as observed using the metal-modulated epitaxy (MME) growth method. 17-20) The use of the lowtemperature (600 °C) MME technique reduces the incorporation of nitrogen vacancies and donor-like defects accountable in part for the hole compensation. This makes MME a promising growth method to achieve low-resistance TJs.

In this work, TJ contacted cells were formed using a hybrid growth approach in which the active solar cell regions were grown by MOCVD and the subsequent homojunction GaN TJ contacts were grown by MBE. Different device types such as LEDs and laser diodes were reported to be obtained using this hybrid growth method^{21,22)} by the regrowth of n-type

¹Georgia Institute of Technology, Atlanta, GA 30332, U.S.A.

²Arizona State University, Tempe, AZ 85280, U.S.A.

³PhotoNitride Devices Inc., Tempe, AZ 85284, U.S.A.

layers via MBE. However, in this work, different TJ structures with a range of p^+/n^+ GaN layer combinations and varied doping levels were grown on top of the MOCVD-grown p^+ GaN contact layers of InGaN/GaN multi-quantum well (MQW) solar cells to draw a conclusion about the optimum TJ contact design.

The cell structure consists of a 1.0 μ m n-GaN (Si \approx 1 \times $10^{17} \, \text{cm}^{-3}$) buffer layer, a 4.5 µm n-GaN (Si $\approx 6 \times 10^{18} \, \text{cm}^{-3}$) n-contact layer, followed by the MQW region composed of a 20-period InGaN (3.0 nm)/GaN (5.6 nm) MQW structure with an In mole fraction of $\sim 13.7\%$, determined by X-ray diffraction (XRD), and a photoluminescence peak emission line at $460 \, \text{nm}$ ($\sim 2.7 \, \text{eV}$). The MQW active region was then followed by a 150-nm-thick GaN:Mg layer ($\sim 2 \times 10^{19} \,\mathrm{cm}^{-3}$) and a 10-nm-thick heavily doped GaN:Mg layer ($\sim 1 \times 10^{20}$ cm⁻³). The Hall acceptor concentration (N_A) of p⁺GaN was measured to be $\sim 2 \times 10^{18}$ cm⁻³.²³⁾ After the MOCVD growth, the Mg atoms were activated at 810 °C under a N2-rich environment for 10 min. It is worth mentioning that, although the growth of the entire InGaN cell with a TJ contact is possible by MOCVD, the thermal activation of buried Mg becomes difficult. H atoms can easily migrate in p-GaN as the binding energy of an electrically neutral Mg acceptor and a H donor is ~0.7 eV,²⁴⁾ whereas the high diffusion barrier of H in n-type GaN (~3.4 eV) renders H almost immobile in n-GaN.²⁵⁾ The lateral out-diffusion of H from the side mesa walls is possible with a dramatic reduction in etched mesa size (e.g., µLEDs), a longer thermal annealing time, and a higher annealing temperature. 4,16) Nevertheless, the active area of solar cell needs to be sufficiently large to efficiently collect the photogenerated carriers, making the lateral diffusion of H challenging. Thus, the hybrid regrowth of InGaN cells with a TJ can be a suitable option to avoid the mentioned challenges.

Generally, the surfaces of MOCVD-grown cells, prior to the MBE regrowth, contain carbon, oxygen, and impurities that can act as unintentional dopants. Various surface treatment methods have been reported to minimize the effect of impurities on carrier transport. ^{26,27)} In this study, the activated cells were treated with a 49% HF solution for 1 min at room temperature prior to loading into the MBE chamber. The HF solution was found to produce the lowest series resistance, compared with H₂SO₄:H₂O₂, HCl, and HNO₃:HCl solutions. After loading into the MBE growth chamber, the cells were thermally out-gassed in situ at 700 °C for 20 min. The subsequent TJ contacts were then grown via shutter pulsing of Ga and Si. Mg and nitrogen plasmas were kept unshuttered. No polarity inversion was observed during the growth.

Sample N consists of MBE-grown n⁺⁺ (20 nm)/n (130 nm)/n⁺ (20 nm) GaN layers with Si concentrations of \sim 4 × 10^{20} , 1×10^{19} , and 4×10^{19} cm⁻³, respectively, in series with the MOCVD-grown p⁺GaN layer (see Fig. 1). All the Si and Mg concentrations in this work were measured by secondary ion mass spectroscopy (SIMS). To effectively increase the tunneling probability, N_A at the junction was increased by preparing an additional sample (P/N), in which a 20-nm-thick p⁺⁺GaN layer (Mg \approx 3 × 10^{20} cm⁻³) was deposited on top of the MOCVD-grown p⁺GaN layer, followed by n-GaN layers with a similar structure to sample N. The highly doped n⁺⁺ and p⁺⁺GaN show Hall carrier concentrations of 3×10^{20} and 1.5×10^{20} cm⁻³ and resistivities of 2×10^{-4} and 0.1Ω cm², respectively.

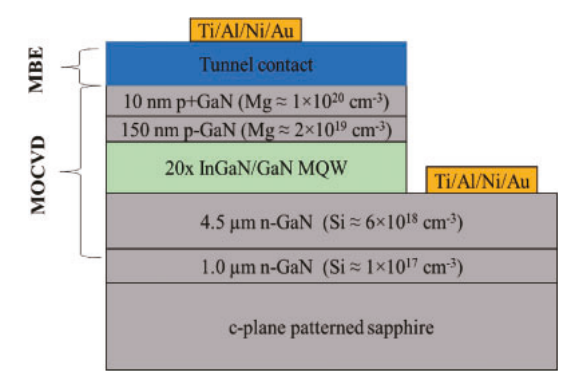


Fig. 1. Device structure of an InGaN/GaN cell with a TJ contact. The tunnel contact layer represents four different structures.

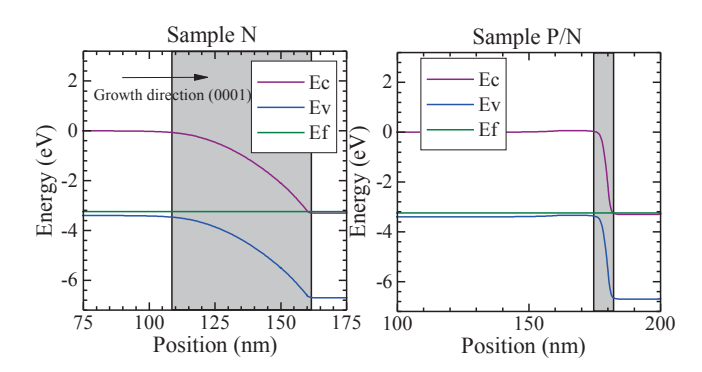


Fig. 2. Band diagrams of the TJ portion of samples N and P/N. The approximated depletion regions are indicated by the shaded areas.

To gain insight into the location and estimated depletion width of the grown TJs, the band alignments of samples N and P/N were calculated using a one-dimensional modeling program (Nextnano³) at room temperature (see Fig. 2).²⁸⁾ The simulated band diagrams at zero applied voltage show that the depletion width of the TJ has been reduced from \sim 41 nm in sample N to \sim 6 nm in sample P/N. The tunneling probability in a p-n junction can be expressed by the Wentzel-Kramers-Brillouin (WKB) approximation²⁹⁾

$$T_{\rm t} \approx \exp\left(-2\int_0^{W_{\rm d}} \sqrt{\frac{2m^* E_{\rm g} x}{\hbar^2 q W_{\rm d}}} dx\right),$$
 (1)

where q is the electron charge, \hbar is the reduced Planck's constant, W_d is the depletion width, E_g is the GaN bandgap $(3.42 \,\mathrm{eV})$, and m^* is the effective mass. Sample P/N shows a band-to-band tunneling probability of $\sim 10^{-15}$. This implies that, even at the high doping concentrations achieved via MME, the direct band-to-band tunneling (Esaki tunneling) is still improbable. Similarly, polarization-assisted tunneling with W_d equal to the interlayer thickness yields low values of 10^{-11} for GaN/AlN (2.6 nm)/GaN and 10^{-18} for GaN/ In_{0.3}Ga_{0.7}N (6 nm)/GaN.^{8,9)} The probable mechanism for the tunneling, particularly in the wide-bandgap materials, is suggested to be defect-assisted tunneling (DAT) through buried impurities in the depletion region, such as Mg precipitates, oxygen contaminants, and deep-level defects acting as carrier traps (e.g., nitrogen vacancies and antisite defects in p-GaN and Ga vacancies in n-GaN).30-33) The presence of DAT in GaN-based diodes was suggested as an explanation for their high ideality factors (n > 2) measured from their current-voltage (I-V) characteristics. ³⁴⁻³⁶⁾ The

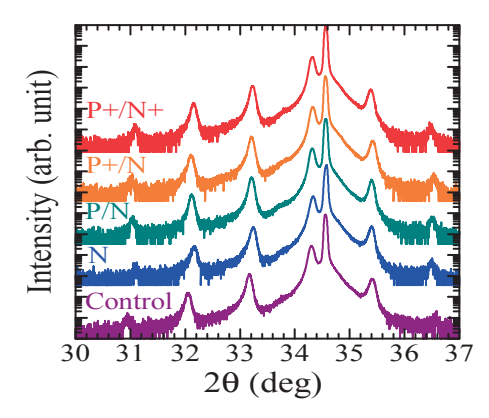


Fig. 3. (0002) 2θ – ω diffraction scans showing the absence of phase separation.

effect of DAT has also been reported in AlGaN/GaN resonant tunneling diodes.³⁷⁾

To further reduce $W_{\rm d}$ and $T_{\rm t}$ through the defective states at the junction, $^{38,39)}$ two additional cells were prepared, which were similar to sample P/N, but with thin highly doped GaN interlayers sandwiched between the MBE-grown n⁺⁺GaN and p⁺⁺GaN layers. Sample P+/N contains an additional 5-nm-thick p⁺⁺⁺GaN layer (Mg $\approx 7 \times 10^{20}\,{\rm cm^{-3}}$) and sample P+/N+ has 5-nm-thick p⁺⁺⁺ (Mg $\approx 7 \times 10^{20}\,{\rm cm^{-3}}$)/9-nm-thick n⁺⁺⁺GaN (Si $\approx 7 \times 10^{20}\,{\rm cm^{-3}}$) interlayers. The Mg doping level is expected to be well beyond the solid solubility of Mg in GaN. However, it is possible to overcome this thermodynamic limitation by kinetically "trapping" Mg into the lattice by the low-temperature MME growth method, resulting in metastable supersaturation acceptors. ¹⁹⁾

As shown in Fig. 3, XRD 2θ – ω scans in the vicinity of (0002) reflections of all samples show superlattice features with a period of ~8.5 nm and the absence of indium phase separation. The control cell refers to a separate MOCVD-grown cell with the p⁺GaN top layer. The AFM images of the hybrid cells show smooth surfaces with spiral hillock features, indicative of step flow growth, with an RMS roughness of <0.5 nm, comparable to that of the control cell (see Fig. 4).

All hybrid samples were fabricated into solar cells with an active area of $\sim 0.56 \,\mathrm{mm}^2$. Standard photolithography and plasma dry etching (BCl₃/Cl₂) processes were performed to electrically isolate individual cells. Metal contacts to n-GaN layers were deposited via e-beam evaporation using Ti/Al/ Ni/Au. The control cell was fabricated using ITO (150 nm) with a sheet resistance of $\sim 50 \Omega/\text{sq}$ as the p-GaN lateral conduction layer and Ti/Pt/Au as metal gridlines on the ITO layer. The ITO layer was deposited by e-beam evaporation with an excess oxygen flow and post-thermal annealing at 500 °C under N₂ atmosphere for 10 min, which was previously found to optimize the resistivity vs absorption trade-off. Details of the growth and fabrication of the control cell can be found in our previous works. ^{23,41)} Owing to the high carrier concentrations achieved via MME, the deposited TJ contacts show ohmic behavior without any thermal annealing.

The dark current density-voltage (*DJ-V*) characteristics of the hybrid and control cells are depicted in Fig. 5(a). The hybrid cells have 5 to 6 orders of magnitude of rectification between -1 and 3 V, showing a reduced turn-on voltage with increased Si and Mg doping levels in the TJ. At a current density of 40 mA/cm², the combined solar cell/TJ forward

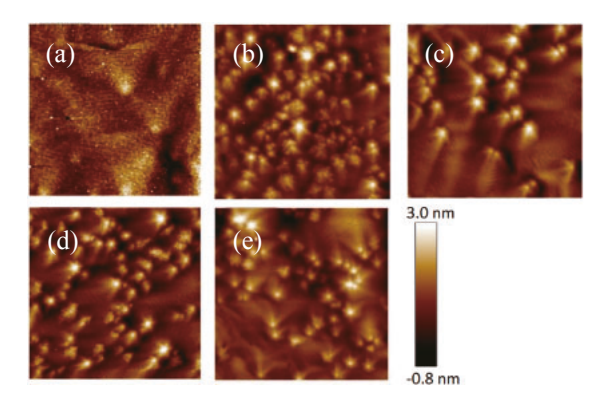


Fig. 4. $5 \times 5 \,\mu\text{m}^2$ AFM images of (a) control cell and samples (b) N, (c) P/N, (d) P+/N, and (e) P+/N+.

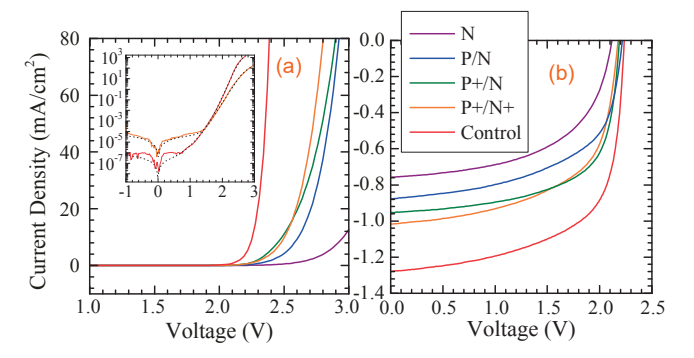


Fig. 5. (a) *DJ–V* and (b) *LJ–V* characteristics of all samples.

bias voltage (in which the TJ is reverse-biased) was measured to be 3.5, 2.8, 2.74, and 2.68 V for samples N, P/N, P+/N, and P+/N+, respectively, compared with 2.4 V for the control cell. These values indicate that, as the doping levels at the junction increase, the voltage drop decreases and the turn-on voltage of the diode also decreases [see Fig. 5(a)]. Sample P+/N+ shows the lowest slope/intercept extrapolated turn-on voltage of ~2.58 V, compared with ~2.32 V for the control cell. We ascribed the low added voltage drop to the extremely high Mg and Si doping levels and the abrupt junction enabled by MME.

By comparing the slopes of DJ-V curves of samples N and P/N at forward bias, it was demonstrated that the overall device series resistance is reduced by depositing the MBEgrown p-doped GaN layer on top of the MOCVD-grown p⁺GaN layer. The specific on-resistance is further reduced by inserting the highly doped GaN interlayers. The *DJ–V* curves of sample P+/N+ and the control cell were fit to a doublediode model to gain more insight into the effect of the TJ on solar cell carrier transport [see the inset of Fig. 5(a)]. The extracted shunt resistances for sample P+/N+ and the control cell are $\sim 1.8 \times 10^6$ and $1.6 \times 10^6 \text{ k}\Omega \text{ cm}^2$, respectively, indicating no significant shunting issues in the hybrid cell. However, the series resistance of sample P+/N+ $(3.2 \,\Omega\,\text{cm}^2)$ is higher than that of the control cell $(0.08 \,\Omega\,\text{cm}^2)$, which implies a higher carrier transport loss in sample P+/N+. The first ideality factor (n_1) of both cells is ~ 2 , which is commonly attributed to the recombination in the depletion region and is expected in a MQW solar cell. In addition, the second ideality factors (n_2) of sample P+/N+ and the control cell are higher, showing values of 3.4 and 5.1, respectively, which corroborate the presence of the DAT mechanism.

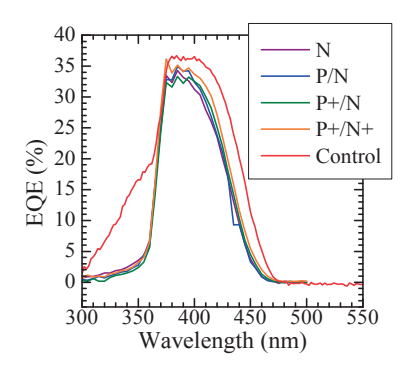


Fig. 6. EQE characteristics of all hybrid cells and the control cell.

Table I. Electrical characteristics of InGaN hybrid and control cells. $W_{\rm OC} \equiv (E_{\rm g}/q) - V_{\rm OC} = {\rm bandgap\text{-}voltage}$ offset.

Sample ID	$J_{\rm SC}$ (mA/cm ²)	V _{OC} (V)	FF (%)	η (%)	W _{OC} (V)
N	0.76	2.0	59	0.90	0.95
P/N	0.88	2.22	57	1.11	0.73
P+/N	0.94	2.22	64	1.34	0.73
P+/N+	1.02	2.2	59	1.32	0.75
Control	1.28	2.24	64	1.82	0.71

The one-sun light J-V (LJ-V) characteristics of all cells were acquired using an AM1.5G Oriel class A solar simulator [see Fig. 5(b) and Table I]. The open-circuit voltage (V_{OC}) of sample N (~2.0 V) is lower than that of the control cell (2.24 V), which can be related to its higher dark current density, originating mainly from the defective regrown junction centered metallurgically in the TJ. However, all other hybrid cells where the p-region was first regrown show similar $V_{\rm OC}$ values (~2.2 V) to the control cell, indicating that the MBE growth of the p-n TJ itself does not degrade the crystal quality or increase the leakage current. Sample P/N shows a higher short-circuit current density (J_{SC}) (0.88 mA/cm^2) than sample N (0.76 mA/cm^2). This can be attributed to the shorter tunneling distance of sample P/N enabled by its higher N_A and reduced density of contaminants at the interface. However, the highly optimized control cell exhibits the highest J_{SC} (1.28 mA/cm²). Compared with samples N and P/N, $J_{\rm SC}$ was increased to 0.94 and 1.02 mA/cm^2 in samples P+/N and P+/N+, respectively, indicating a higher relative carrier collection achieved by using the heavily doped GaN interlayers. This may be due to the slightly greater band bending induced by the heavily doped layers, effectively reducing the tunneling distance and possibly increasing the DAT contribution to the carrier transport. It can be concluded that the presence of highly doped layers at the junction can improve the electrical performance of the TJ and cell.

Since the TJ is critical for the success of future tandem solar cells and yet these first TJ connected devices underperform the optimized control sample, it is critical to understand where the loss originates. The measured external quantum efficiency (EQE) shown in Fig. 6 provides some insights. The main spectral response of all hybrid cells occurs in the range of 360–460 nm. In the low-wavelength regime (300–360 nm), the control cell exhibits higher EQE values than the hybrid cells, as the EQE of the hybrid cells is

sharply reduced below ~365 nm. This drop in EQE is due to the presence of thick and highly doped MBE-grown top layers with strong absorption at short wavelengths. For instance, for sample N with an added 170 nm of regrown n-type GaN, an absorption depth calculation based on the wavelength-dependent extinction coefficient of GaN reveals that >80% of photons with a wavelength greater than 350 nm will be absorbed⁴²⁾ before reaching the active layers. Thus, the thickness of the TJ is higher than the penetration depth of the low-wavelength photons and needs to be reduced to avoid the parasitic loss.

Conversely, the lower EQE values at the peak and at long wavelengths in the hybrid cells compared with the control cell are not inherent to the TJ but are associated with the indium fluctuation in the InGaN/GaN QWs of the control cell. The band gaps acquired from the inflection points of the EQE data at long wavelengths for the hybrid and control cells are ~ 2.88 and 2.82 eV, respectively, which implies a higher In content in the control cell (verified by XRD).

In addition, although the surface treatment was effective, the presence of contaminants at the interface can still hinder the effective carrier transport through p-regrown layers prior to the TJ. A thin n-doped contaminant sheet charge at the regrowth interface between the MOCVD p⁺GaN and MBE p⁺⁺GaN layers can cause band bending and acts as a barrier to hole extraction. Thus, the regrowth interface is a major limitation in the ultimate utilization of hybrid TJs for solar cells.²⁶⁾

In conclusion, solar cells with low-resistance p–n GaN homojunction tunnel contacts were grown via a hybrid MOCVD/MBE method. Increasing the Mg and Si concentrations of the TJ reduces the turn-on voltage of the diode giving a low voltage drop across the TJ. The best InGaN MQW solar cell with a TJ contact show $V_{\rm OC}$ and $J_{\rm SC}$ values of 2.2 V and 1.02 mA/cm², respectively, comparable to those of the control cell with a traditional top contact based on ITO.

Acknowledgment This work was funded in part by the Advanced Research Projects Agency Energy, U.S. Department of Energy, under Award Number DE-AR0000470.

- E. A. Clinton, E. Vadiee, C. A. M. Fabien, M. W. Moseley, B. P. Gunning, W. A. Doolittle, A. M. Fischer, Y. O. Wei, H. Xie, and F. A. Ponce, Solid-State Electron. 136, 3 (2017).
- C. A. M. Fabien, A. Maros, C. B. Honsberg, and W. A. Doolittle, IEEE J. Photovoltaics 6, 460 (2016).
- 3) J. Wu, J. Appl. Phys. 106, 011101 (2009).
- D. Hwang, A. J. Mughal, M. S. Wong, A. I. Alhassan, S. Nakamura, and S. P. DenBaars, Appl. Phys. Express 11, 012102 (2018).
- S.-R. Jeon, Y.-H. Song, H.-J. Jang, G. M. Yang, S. W. Hwang, and S. J. Son, Appl. Phys. Lett. 78, 3265 (2001).
- 6) J. Boucart, C. Starck, F. Gaborit, A. Plais, N. Bouche, E. Derouin, J. C. Remy, J. Bonnet-Gamard, L. Goldstein, C. Fortin, D. Carpentier, P. Salet, F. Brillouet, and J. Jacquet, IEEE J. Sel. Top. Quantum Electron. 5, 520 (1999).
- M. T. Hardy, C. O. Holder, D. F. Feezell, S. Nakamura, J. S. Speck, D. A. Cohen, and S. P. Denbaars, Appl. Phys. Lett. 103, 081103 (2013).
- S. Krishnamoorthy, D. N. Nath, F. Akyol, P. S. Park, M. Esposto, and S. Rajan, Appl. Phys. Lett. 97, 203502 (2010).
- J. Simon, Z. Zhang, K. Goodman, H. Xing, T. Kosel, P. Fay, and D. Jena, Phys. Rev. Lett. 103, 026801 (2009).
- 10) S. Krishnamoorthy, F. Akyol, P. S. Park, and S. Rajan, Appl. Phys. Lett. 102, 113503 (2013).
- 11) J. M. O. Zide, A. Kleiman-Shwarsctein, N. C. Strandwitz, J. D. Zimmerman, T. Steenblock-Smith, A. C. Gossard, A. Forman, A. Ivanovskaya, and G. D. Stucky, Appl. Phys. Lett. 88, 162103 (2006).
- 12) S. Krishnamoorthy, T. F. Kent, J. Yang, P. S. Park, R. C. Myers, and S. Raian, Nano Lett. 13, 2570 (2013).

- 13) M. Diagne, Y. He, H. Zhou, E. Makarona, A. V. Nurmikko, J. Han, K. E. Waldrip, J. J. Figiel, T. Takeuchi, and M. Krames, Appl. Phys. Lett. 79, 3720 (2001).
- 14) I. Ozden, E. Makarona, A. V. Nurmikko, T. Takeuchi, and M. Krames, Appl. Phys. Lett. 79, 2532 (2001).
- 15) E. A. Clinton, E. Vadiee, S.-C. Shen, K. Mehta, P. D. Yoder, and W. A. Doolittle, Appl. Phys. Lett. 112, 252103 (2018).
- 16) F. Akyol, S. Krishnamoorthy, Y. Zhang, J. Johnson, J. Hwang, and S. Rajan, Appl. Phys. Lett. 108, 131103 (2016).
- 17) B. Gunning, J. Lowder, M. Moseley, and W. A. Doolittle, Appl. Phys. Lett. 101, 082106 (2012).
- 18) G. Namkoong, E. Trybus, K. K. Lee, M. Moseley, W. A. Doolittle, and D. C. Look, Appl. Phys. Lett. 93, 172112 (2008).
- 19) B. P. Gunning, C. A. M. Fabien, J. J. Merola, E. A. Clinton, W. A. Doolittle, S. Wang, A. M. Fischer, and F. A. Ponce, J. Appl. Phys. 117, 045710 (2015).
- M. Moseley, B. Gunning, J. Lowder, W. A. Doolittle, and G. Namkoong, J. Vac. Sci. Technol. B 31, 03C104 (2013).
- 21) S. Golka, C. Pflügl, W. Schrenk, G. Strasser, C. Skierbiszewski, M. Siekacz, I. Grzegory, and S. Porowski, Appl. Phys. Lett. 88, 172106 (2006).
- 22) B. P. Yonkee, E. C. Young, C. Lee, J. T. Leonard, S. P. Denbaars, J. S. Speck, and S. Nakamura, Opt. Express 24, 7816 (2016).
- 23) J. J. Williams, H. McFavilen, A. M. Fischer, D. Ding, S. Young, E. Vadiee, F. A. Ponce, C. Arena, C. B. Honsberg, and S. M. Goodnick, IEEE J. Photovoltaics 7, 1646 (2017).
- 24) J. Neugebauer and C. G. Van de Walle, Phys. Rev. B 50, 8067 (1994).
- 25) C. G. Van de Walle, C. Stampfl, and J. Neugebauer, J. Cryst. Growth 189–190, 505 (1998).
- 26) S. Chowdhury, M. H. Wong, B. L. Swenson, and U. K. Mishra, IEEE Electron Device Lett. 33, 41 (2012).
- 27) B. P. Yonkee, E. C. Young, S. P. DenBaars, S. Nakamura, and J. S. Speck, Appl. Phys. Lett. 109, 191104 (2016).

- S. Birner, T. Zibold, T. Andlauer, T. Kubis, M. Sabathil, A. Trellakis, and P. Vogl, IEEE Trans. Electron Devices 54, 2137 (2007).
- 29) S. M. Sze and K. K. Ng, *Physics of Semiconductor Devices* (Wiley, New York, 2007).
- K. Sakowski, L. Marcinkowski, S. Krukowski, S. Grzanka, and E. Litwin-Staszewska, J. Appl. Phys. 111, 123115 (2012).
- 31) J. B. Fedison, T. P. Chow, H. Lu, and I. B. Bhat, Appl. Phys. Lett. 72, 2841 (1998)
- 32) M. Auf der Maur, B. Galler, I. Pietzonka, M. Strassburg, H. Lugauer, and A. Di Carlo, Appl. Phys. Lett. 105, 133504 (2014).
- 33) E. C. Young, B. P. Yonkee, F. Wu, S. H. Oh, S. P. DenBaars, S. Nakamura, and J. S. Speck, Appl. Phys. Express 9, 022102 (2016).
- 34) A. Chitnis, A. Kumar, M. Shatalov, V. Adivarahan, A. Lunev, J. W. Yang, G. Simin, M. A. Khan, R. Gaska, and M. Shur, Appl. Phys. Lett. 77, 3800 (2000).
- M. Binder, B. Galler, M. Furitsch, J. Off, J. Wagner, R. Zeisel, and S. Katz, Appl. Phys. Lett. 103, 221110 (2013).
- 36) P. Perlin, M. Osiński, P. G. Eliseev, V. A. Smagley, J. Mu, M. Banas, and P. Sartori, Appl. Phys. Lett. 69, 1680 (1996).
- C. Bayram, Z. Vashaei, and M. Razeghi, Appl. Phys. Lett. 97, 181109 (2010).
- 38) H. Okumura, D. Martin, M. Malinverni, and N. Grandjean, Appl. Phys. Lett. 108, 072102 (2016).
- C. Bayram, Z. Vashaei, and M. Razeghi, Appl. Phys. Lett. 97, 092104 (2010)
- 40) F. Bernardini, V. Fiorentini, and A. Bosin, Appl. Phys. Lett. 70, 2990
- 41) J. J. Williams, H. McFavilen, A. M. Fischer, D. Ding, S. R. Young, E. Vadiee, F. A. Ponce, C. Arena, C. B. Honsberg, and S. M. Goodnick, Conf. Rec. IEEE Photovoltaic Specialists Conf., 2016.
- 42) T. Kawashima, H. Yoshikawa, S. Adachi, S. Fuke, and K. Ohtsuka, J. Appl. Phys. 82, 3528 (1997).